Planar Porous THz Waveguides for Low-Loss Guidance and Sensing Applications

Andrey Markov, Anna Mazhorova, and Maksim Skorobogatiy

Abstract—**Planar porous dielectric waveguides featuring periodic sequence of deeply subwavelength air/dielectric bi-layers are proposed, fabricated and characterized in view of their potential applications as low-loss waveguides and sensors in the THz spectral range. The waveguide design maximizes the fraction of power guided in the air to reduce waveguide loss due to material absorption, as well as to provide a conveniently accessible microfluidic channels for sensor measurements.**

Index Terms—**Frequency domain, numerical modeling, terahertz (THz), waveguides.**

I. INTRODUCTION

THE main complexity in designing terahertz waveguides is the fact that almost all materials are highly absorbent in the terahertz region [1]. Since the lowest absorption loss occurs in dry air, an efficient waveguide design must maximize the fraction of power guided in the air. Different types of THz waveguides and fibers have been proposed based on this concept. The simplest subwavelength fiber [2]–[4], features dielectric core that is much smaller than the wavelength of guided light. As a result, a high fraction of modal power is guided outside of the lossy material and in the low-loss gaseous cladding. Another type of low-loss fibers features porous core region with the size of the individual pores much smaller than the wavelength of light [2], [3]. As a result, guided light is concentrated mostly in the low-loss gas-filled pores inside the core and in the gaseous cladding. Porous fibers, generally, feature higher confinement in the core region and are less prone to bending losses and influence of the environment compared to simple rod-in-the-air subwavelength fibers [2], [7]. Another important type of the low-loss waveguides feature hollow gas-filled core surrounded by a structured cladding serving as a reflector. The main challenge in the design of such waveguides is to ensure high reflection at the core-cladding interface. Different hollow-core structures have been investigated including metalized bores [5]–[7], periodic dielectric multilayers [8], as well as thin-walled dielectric pipes [9]–[11]. Other types of the THz waveguide are parallel plate waveguides [12] and slit waveguides [13] remarkable for their low transmission losses and high mode confinement. Metal wire, can be used to transport terahertz pulses with virtually no dispersion and low attenuation [14].

In this paper we explore a novel design of a planar porous low-loss waveguide for 0.1–1.5 THz frequency range. The waveguide structure consists of multiple layers of thin (25–50 μm) polyethylene film that are separated by low-loss air layers of comparable thickness. We believe that waveguides described in this paper can be useful not only for low-loss THz wave delivery but also for sensing of biological and chemical specimens in the terahertz region by placing the recognition elements directly into the waveguide microstructure similarly to what has been recently demonstrated in [15].

The main advantage of the proposed planar porous waveguides is the convenient access to their optical mode, since the major portion of THz power launched into such a waveguide is confined within the air layers. Moreover, small spacing between the layers promotes rapid loading of the analyte into the waveguide due to strong capillary effect ($<$1 s filling of a 10 cm long waveguide with an analyte). The modal refractive index of porous waveguide is smaller compared to pure polymer and it is easy to adjust by changing the air spacing between the layers, as well as the number of layers in the core. The porous waveguide exhibits considerably smaller transmission losses than a bulk material. For completeness we note that planar multilayered materials have been recently studied in a broader context of birefrigent anisotropic materials for THz devices [16].

II. WAVEGUIDE DESIGN

The photograph of a planar porous multilayer waveguide and its metal holder is presented in the Fig. 1(a). The waveguide has been fabricated using commercial 50 μm thick polyethylene films. The layers were stacked together and separated using spacers in the form of a plastic tape placed along the waveguide edges. The layers and the spacers were held together by metal holders that also allowed some tension control over the whole structure, thus, resulting in a porous core with well-defined and consistent 75 μm air gaps between the individual polyethylene layers. The thickness of the spacers has been measured with the optical microscope to be 75 μm [see Fig. 1(b)], the tension of the polyethylene layers has been high enough to maintain the uniform thickness of the air layers. The overall width of a THz waveguide is 3.3 cm and its length is 11 cm. The number of polyethylene layers used in our experiments varied from 1 to 10, with the maximal core thickness of 1.2 mm (10 layers). The influence of the metal borders of the waveguide on its optical properties will be discussed later in the paper.

As the major portion of the THz light propagating in such planar porous waveguides is confined within the low-loss air layers, the relatively high absorption loss of Polyethylene films are effectively mitigated. Moreover, the waveguide optical
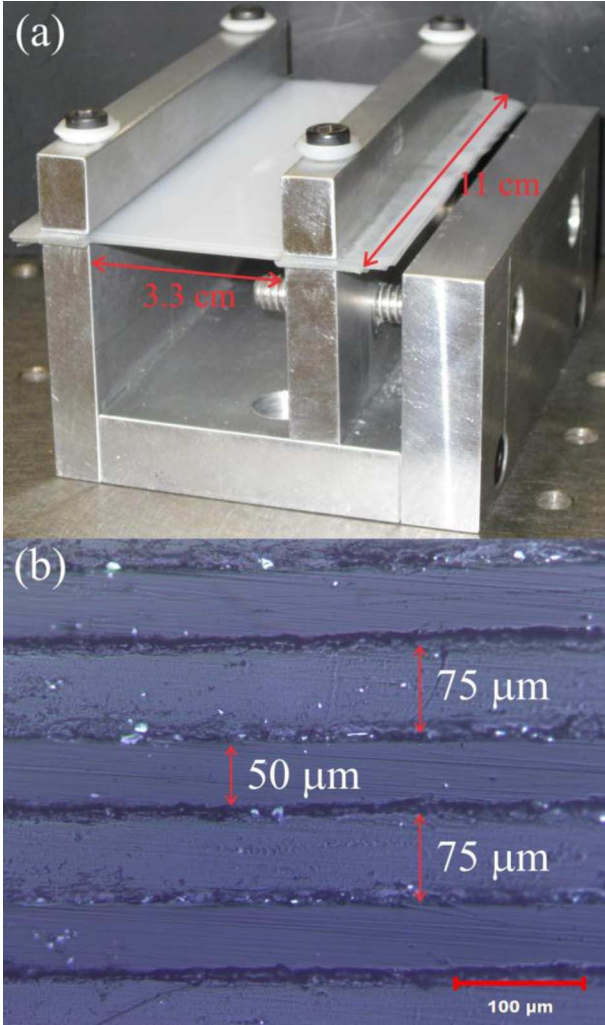
Fig. 1. (a) Photograph of the planar porous multilayer waveguide fabricated from polyethylene and its metal holder. (b) Microscope image of the waveguide cross-section (in the place where the PE layers are separated by the spacers), the thickness of the polyethylene layers is 50 μm, while the thickness of spacers is 75 μm.

properties are very sensitive to the real and imaginary parts of the permittivity of the separating (air) layers, thus, making it possible to use changes in the waveguide transmission spectrum for characterizing of the specimens placed inside of the waveguide structure (such as gases and liquids).

III. FUNDAMENTAL MODE OF THE WAVEGUIDE

The multilayer porous waveguides features a broader spectral region of single mode operation compared to the fully solid slab waveguide of the same size. The criterion for a single mode operation of a planar slab waveguide is [17]

$$k \cdot d \cdot \sqrt{n_2^2 - n_1^2} < \pi \qquad (1)$$

where n_2 is the refractive index of the core material, which for most materials is larger than $n_2 > 1.45$, and n_1 is the refractive index of the cladding material, which in our case equals to $n_1 = 1$, d is the thickness of the slab waveguide. Thus, for
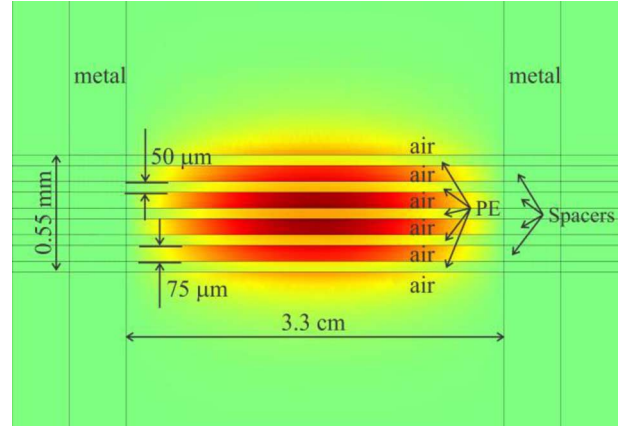

Fig. 2. Transverse electric field distribution of the fundamental mode of the porous waveguide.

single mode propagation for most practical materials the single mode operation criterion is $d < \lambda/2$. On the other hand, the waist size of the Gaussian beam of the source depends on the radiation wavelength. The theory predicts and the conducted experiments confirm that the diameter of the Gaussian beam used in our experiments is directly proportional to the operation wavelength. Particularly, in our THz setup we have measured that beam FWHM is about $2.5 \cdot \lambda$. For high coupling efficiency the waveguide width should be comparable to the waist of the source beam, and hence, $d \sim 2.5 \cdot \lambda$, which contradicts the above mentioned criterion for single mode propagation in a solid slab waveguide. Thus, in a single slab waveguide single mode operation usually comes at a price of a very low excitation efficiency of the fundamental core mode.

In a stark contrast with solid slab waveguides, the multilayer porous waveguide can be designed to be arbitrarily large in size and still guide only a single mode. Particularly, in the porous waveguides where higher refractive index (solid) layers of refractive index are separated with lower refractive index (air) layers (assumed to be of the same material as the cladding), then single mode operation condition becomes [17]

$$k \cdot d \cdot \sqrt{n_2^2 - n_1^2} \sqrt{\delta_2} < \pi \qquad (2)$$

where $\delta_2 = d_{\mathrm{solid}}/(d_{\mathrm{solid}} + d_{\mathrm{air}})$ is the relative size of the solid layers in the solid/air bilayer and d is the total height of the waveguide. This expression is derived in the limit when both the solid and air layers are deeply subwavelength. For the transverse electric field distribution of the fundamental mode of the porous waveguide see Fig. 2. For the single mode criterion in terms of the waveguide size we then get

$$d < \lambda \left/ \left(2 \sqrt{n_2^2 - n_1^2} \sqrt{\delta_2} \right) \right. \qquad (3)$$

Thus, by choosing a small enough relative size of the higher refractive-index layers we can make increase the transverse size of the waveguide to the required lever while preserving its single mode guiding regime.

IV. DETAILS OF THE NUMERICAL MODELING OF THE MODAL FIELDS

In the following sections we explain the transmission features of planar porous waveguides using semi-analytical theoretical model. In what follows, the distribution of the transverse E-field components $\vec{E}_{\text{output}} = (E_{\text{output}}^x, E_{\text{output}}^y)$ at the output facet of a waveguide of length L_w is modeled as the coherent superposition of the N guided modes

$$
\begin{aligned}
&\vec{E}_{\text{output}}(x, y, \omega) \\
&= \sum_{m=1}^{N} C_m \cdot \vec{E}_m(x, y, \omega) \times \exp\left(i\frac{\omega}{c} \cdot n_{\text{eff},m} \cdot L_w\right) \\
&\quad \cdot \exp\left(-\frac{\alpha_m L_w}{2}\right)
\end{aligned}
\tag{4}
$$

where $\vec{E}_{\text{output}} = (E_{\text{output}}^x, E_{\text{output}}^y)$ stands for the transverse field components of the mth guided mode, the x-axis and y-axis correspond to the horizontal and vertical directions in the Fig. 2 and the subsequent figures. The variables α_m and $n_{\text{eff},m}$ denote, respectively, the power loss coefficient and the real effective index of the mth mode at a given frequency ω. The variable C_m refers to the normalized amplitude coupling coefficients computed from the overlap integral of the respective flux distributions of the mth mode with that of the 2D Gaussian beam of the source. Specifically, the definition of C_m is based on the continuity of the transverse field components across the input interface (i.e., cross-section of the subwavelength waveguide) between the incident beam and the excited fiber modes [17]

$$
\begin{aligned}
C_m = &\frac{1}{4} \int_{\text{wc}} dx\,dy (\mathbf{E}_m^*(x, y) \times \mathbf{H}_{\text{Input}}(x, y) \\
&+ \mathbf{E}_{\text{Input}}(x, y) \times \mathbf{H}_m^*(x, y)) \\
&\times \frac{1}{\sqrt{\frac{1}{2}\text{Re} \int_{\text{wc}} dx\,dy\,(\mathbf{E}_m^*(x, y) \times \mathbf{H}_m(x, y))}} \cdot \\
&\times \frac{1}{\sqrt{\frac{1}{2}\text{Re} \int_{\text{wc}} dx\,dy\,\left(\mathbf{E}_{\text{Input}}^*(x, y) \times \mathbf{H}_{\text{Input}}(x, y)\right)}} \cdot
\end{aligned}
\tag{5}
$$

To model the field structure of the source, we assume a y-polarized 2D Gaussian beam along the y-direction and uniform in x-direction whose fields are normalized to carry power P as follows:

$$
\vec{E}_{\text{Input}}(x, y) = \vec{n}_x \cdot \sqrt{\frac{2P}{\pi\sigma^2}} \cdot \exp\left[-\frac{y^2}{2\sigma^2}\right]
\tag{6}
$$

$$
\vec{H}_{\text{Input}}(x, y) = \vec{n}_y \cdot \frac{1}{\sqrt{\mu_0/\varepsilon_0}} \cdot \sqrt{\frac{2P}{\pi\sigma^2}} \cdot \exp\left[-\frac{y^2}{2\sigma^2}\right]
\tag{7}
$$

where the Gaussian beam waist parameter σ is related to the full-width half-maxima by field as $\text{FWHM} = 2\sigma\sqrt{2 \cdot \ln 2}$, $\vec{n}_x$ and $\vec{n}_y$ are unit vectors, and $\sqrt{\mu_0/\varepsilon_0}$ is the intrinsic impedance of vacuum. The frequency dependence of the beam waist was measured independently and then fitted by a linear function of the input wavelength with a result $\sigma \approx 2.5 \cdot \lambda$. This model was subsequently used in the following simulations.
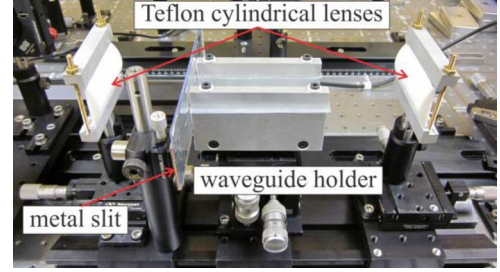

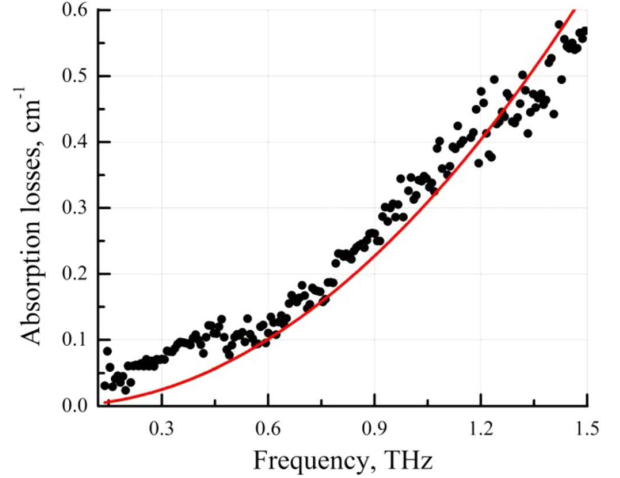Fig. 3. Experimental THz–TDS setup with the waveguide fixed between two cylindrical teflon lenses.

Fig. 4. Absorption losses of the bulk polyethylene. Red line—quadratic fitting curve.

V. MEASUREMENT SETUP

All the data in our experiments was acquired using a modified THz-TDS (Time-Domain Spectroscopy) setup. The setup consists of a frequency-doubled femtosecond fiber laser (MenloSystems C-fiber laser) used as a pump source and identical GaAs dipole antennae used as source and detector yielding a spectrum range ~0.1 to 1.5 THz.

In contrast with a standard arrangement of most THz-TDS setups where the configuration of parabolic mirrors is static, our setup has mirrors mounted on the translation rails. This flexible geometry allows measurement of the waveguides up to 45 cm in length without any realignment. Fig. 3 illustrates the experimental setup where the planar waveguide is placed between the focal lines of the two teflon cylindrical lenses. The cylindrical lenses change the transverse profile of the Gaussian beam from the source by reshaping it into the beam uniform in the direction of the waveguide layers and Gaussian in the perpendicular direction which is then launched into the planar waveguide core. The metal slit before the waveguide input facet is used to avoid propagation along the upper and lower surfaces of the waveguide. The width of the slit is 1.5 mm, which is higher than the major part of the studied wavelength range, thus, the diffraction effects can be significant only for frequencies below 0.2 THz. Slit's dimension was adjusted experimentally so that the spectra measured with and without it are practically the same.
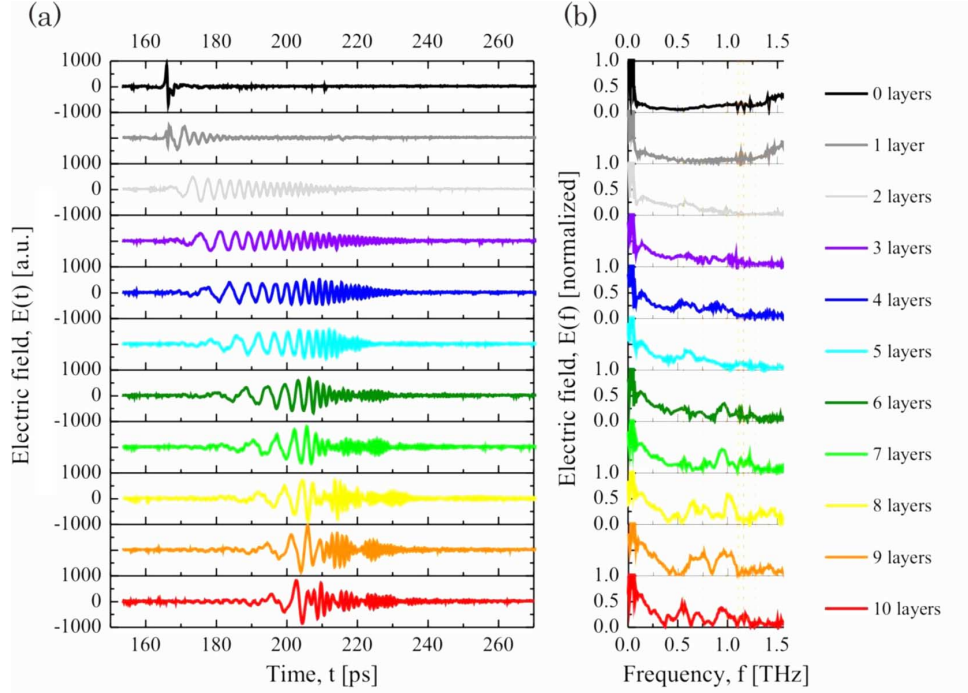
Fig. 5.   Experimentally measured electric field: (a) in time domain and (b) in frequency domain at the output of the waveguide for different number of layers in the waveguide core. Black line corresponds to the absence of the waveguide.

VI. POLYETHYLENE: REFRACTIVE INDEX AND ABSORPTION LOSSES

In order to model the optical properties of the waveguide, first, we have measured the transmission and absorption through the commercial polyethylene (LDPE) bulk material used in the waveguide fabrication. Characterization of refractive index and absorption losses was performed with a THz-time domain spectroscopy (TDS) setup using thick polymer slabs with parallel interfaces. The sample was prepared by cutting and polishing a 1.5 cm thick slice of the PE rod.

The refractive index and absorption losses of polyethylene were retrieved by fitting the predictions of a transfer matrix model to the experimental transmission data [18]. The determined refractive index is largely constant between 0.10 and 1.00 THz and equal to $n_{\mathrm{PE}} = 1.514$. Power absorption losses in cm^{-1} of polyethylene increase quadratically as a function of frequency and can be fitted as $\alpha_{\mathrm{PE,slubs}}$ $\mathrm{cm}^{-1} \approx 0.28 \cdot f^2$ THz (see Fig. 4), where f is the frequency in THz. The absorption losses rapidly increase with frequency, therefore, the propagation length (defined at the $1/e$ of original intensity) in bulk plastic is about 3 m for 0.1 THz frequency and only 3 cm for 1 THz.

Note that polyethylene losses measured using bulk samples (polished slabs from the large diameter cylindrical rods) are typically consistently smaller than the losses of polyethylene films extruded from the same material. We believe that this can be explained by the difference in the surface roughness of polished slabs and films. From experiments we find that losses of thin films can be 2–4 times larger than those of the polished slabs made of the same material. Further studies are necessary to understand this discrepancy. From numerical simulations that

follow we find that the best fit with the experimental data is achieved when absorption losses of the polyethylene films are taken as $\alpha_{PE,\mathrm{films}}$ $\mathrm{cm}^{-1} \approx 0.89 \cdot f^2$ THz.

VII. WAVEGUIDE TRANSMISSION AND DISPERSION MEASUREMENTS

In Fig. 5, we present experimentally measured electric field at the output of the waveguides having different number of layers in the core. Interestingly, we note that increasing the number of layers also increases the bandwidth of the waveguides, from 0.15 to 0.6 THz for a 1-layer waveguide to 0.15–1.5 THz for a 10-layer waveguide. Regardless of the number of layers all the spectra exhibit small oscillations in transmission. Also there are some pronounced dips in the transmission spectra, with their number and depths depending on the number of layers in the waveguide. Thus, there is just one transmission peak for waveguides having 1–3 layers, two transmission peaks for waveguides having 4–6 layers and three peaks for the waveguides with the number of layers larger than 7. As we will see in the upcoming sections, spectral dips signify the onset of multimode guidance for waveguides with larger core sizes (larger number of layers in the core).

Experimentally measured electric field in time domain at the output of the waveguide [see Fig. 5(a)] allows direct measurement of the waveguide dispersion. The dispersion is proportional to the increase of the pulse duration and inversely proportional to the pulse bandwidth and the length of the waveguide. However, it is somewhat difficult to define exactly the starting and finishing points of the pulse, leading to high relative error in the dispersion estimation. The approximate dispersion values extracted from the experimental data don't exceed
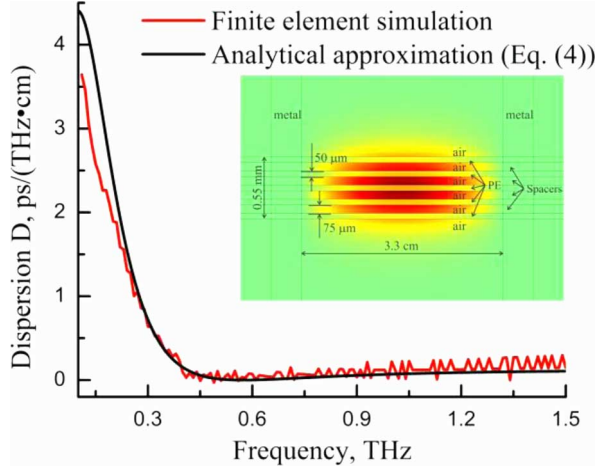
Fig. 6. Dispersion of the fundamental mode of a porous waveguide; comparison between exact simulation and analytical approximation. Black line—analytically calculated dispersion (see (8)), red line—dispersion computed using finite element method. Layer width 50 μm, spacer width 75 μm, overall waveguide size 0.55 mm, 5 PE layers.

1 ps/(THz·cm) which is significantly lower than typical dispersion values for slab waveguides of the comparable dimensions.

Small temporal spreading of the short terahertz pulse is important to maintain high signal-to-noise ratio when transmitting over appreciable distances. Dispersion of the fundamental core mode of the infinite waveguide can be estimated analytically. For a waveguide with size d, having a cladding refractive index n_1, and a porous core made of the two layers with the refractive indices n_2 and n_1, and the relative size of the solid layers in the solid/air bilayer δ_2, the dispersion is [17]

$$D \simeq \frac{1}{c} \frac{\Delta\varepsilon_{\text{porous}}}{4 n_1 \omega} \gamma (1 - \xi\gamma)(3 - 4\xi\gamma) + O\left(\left(\frac{\omega}{\omega_{\text{porous}}}\right)^5\right) \tag{8}$$

where

$$\Delta\varepsilon_{\text{porous}} = \left(n_2^2 - n_1^2\right) \cdot \delta_2; \quad \omega_{\text{porous}} = \frac{c}{d} \frac{1}{\sqrt{\Delta\varepsilon_{\text{porous}}}}$$

$$\xi = \frac{1}{3} + \frac{\Delta\varepsilon_{\text{porous}}}{16 \cdot n_1^2}; \quad \gamma = \frac{\omega^2}{\left(\omega_{\text{porous}}\right)^2 + \xi\omega^2}. \tag{9}$$

Dispersion of the fundamental mode of the waveguide has been also computed using finite element simulation. Effective refractive index of the fundamental mode $n_{\text{eff}}(\omega)$ has been obtained in .COMSOL Multiphysics FEM software and, then, dispersion has been computed

$$D = \frac{1}{c} \frac{\partial^2 \left(n_{\text{eff}}(\omega) \cdot \omega\right)}{\partial \omega^2}. \tag{10}$$

Comparison between waveguide dispersion obtained using two different approaches is presented in Fig. 6 for the waveguide with 5 PE layers and overall thickness 0.55 mm. Fig. 6 shows an excellent match between the analytical and simulated results except for the low frequency region, where it becomes difficult to compute the waveguide mode in FEM software due to strong mode delocalization.

VIII. FITTING EXPERIMENTAL TRANSMISSION DATA WITH A THEORETICAL MODEL

We can now derive an expression for the intensity of the transmitted field as measured by the detector placed at the output facet of a waveguide

$$T(\omega) = \iint\limits_{\text{waveguide}} |\vec{E}_{\text{output}}(x, y, \omega)| \cdot dx\, dy$$

$$= \iint\limits_{\text{waveguide}} \left| \sum_{m=1}^{N} C_m \vec{E}_m(x, y, \omega) \cdot \exp\left(i\frac{\omega n_{\text{eff},m} L_w}{c}\right) \right.$$

$$\left. \cdot \exp\left(-\frac{\alpha_m L_m}{2}\right) \right| \tag{11}$$

To study numerically the propagation in the planar porous waveguides we imported its cross-section into COMSOL Multiphysics FEM software and then solved for the complex effective refractive indices and field profiles. Coupling coefficients were computed for each mode as overlap integrals between the modal fields and the fields of a 2D Gaussian beam. Relative transmission through the waveguide was calculated at the waveguide center using (11) and dividing it by the reference spectrum at waveguide input end.

In the horizontal direction the waveguide core is limited by the metal walls leading to the quantization of the modal wave vector in the transverse direction which is also equivalent to the appearance of the numerous side propagating modes. The nature of the side modes is easy to understand. We first consider an infinite slab waveguide that supports a single mode with refractive index n_0. Note that direction of the mode wave vector $\bar{k}$ can be anywhere in the plane of the waveguide core as long as both of its components satisfy the dispersion relation

$$k_x^2 + k_z^2 = n_0^2 (\omega/c)^2. \tag{12}$$

When confining the mode in the x direction with metallic boundaries, this forces the transverse wave vector component to be quantized

$$k_{x,p} \approx \frac{\pi(p-1)}{W} \tag{13}$$

which is equivalent to the quantization of the propagation directions of the same fundamental mode of a waveguide. W in (13) is the width of the waveguide and $p = 1, 2, 3 \ldots$ is the side mode number. Side modes are thus, nothing else as the same fundamental mode propagation at different angles with respect to the waveguide direction. In (13) the modal index $\text{p} = 1$ corresponds to the mode propagating along the waveguide direction, and its refractive index is typically very close to that of the mode of an infinite planar waveguide. Refractive index of the side modes can be easily derived from the original dispersion relation (12) and the quantization condition (13) as

$$k_{x,p}^2 + k_{z,p}^2 = n_0^2 \left(\frac{\omega}{c}\right)^2$$

$$n_p = \frac{k_{z,p} c}{\omega} = \sqrt{n_0^2 - \left(\frac{c k_{x,p}}{\omega}\right)^2}$$

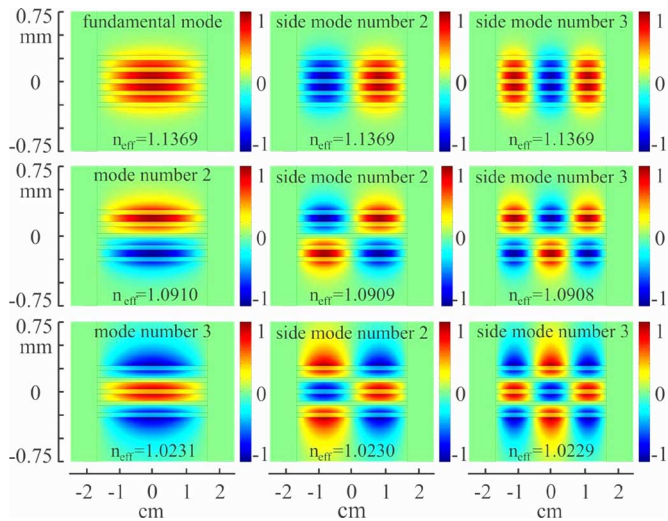$$= \sqrt{n_0^2 - \left(\frac{\lambda(p-1)}{2W}\right)^2} \tag{14}$$

Fig. 7. Transverse electric field distributions of the lower order modes of the waveguide. The modes in the second and third columns are defined as the side modes of the fundamental (top left) and higher order modes (other modes of the first column) in the text of the paper.

where p is the side mode number and W is width of the waveguide. We have verified that a very good agreement between analytical expression for the side mode dispersion relation (14) and results of exact Comsol simulations are observed. Moreover, from the modal filed structure of the 2D Gaussian beam and the field structure of the side modes (see Fig. 7) it is clear that there is a simple approximate relation between the coupling coefficients from the Gaussian beam into the side mode of the p's order. Particularly

$$C_p = \begin{cases} C_1/p, & p = 2n + 1 \\ 0, & p = 2n \end{cases} \qquad (15)$$

where C_1 is the coupling coefficient into the fundamental mode of a metal bounded waveguide. We have verified that this simple analytical relation is in very good correspondence with the results of an exact Comsol simulation.

Comparison of the numerical simulations of spectral transmission through the waveguide to the experimental data is depicted in Fig. 8 for several waveguides having different number of layers in the core region. The presence of small oscillations in the transmission curves can be clearly attributed to the presence of a large number of side modes corresponding to the same mode of an infinite planar waveguide. At the same time, the presence of more pronounced dips in the transmission spectrum can be unambiguously explained by appearance of the higher-order waveguide modes and their destructive interference with the fundamental mode of a waveguide in the vicinity of their cutoff frequencies due to large mismatch in their effective refractive indices. Overall, we observe a good comparison between experimental and numerical results.

IX. CONCLUSION

Planar porous waveguides featuring a periodic sequence of the subwavelength material layers separated with air regions are proposed as waveguides for THz radiation. A large fraction of the modal fields in these waveguides is guided in the low-loss air region, thus effectively reducing the waveguide transmission
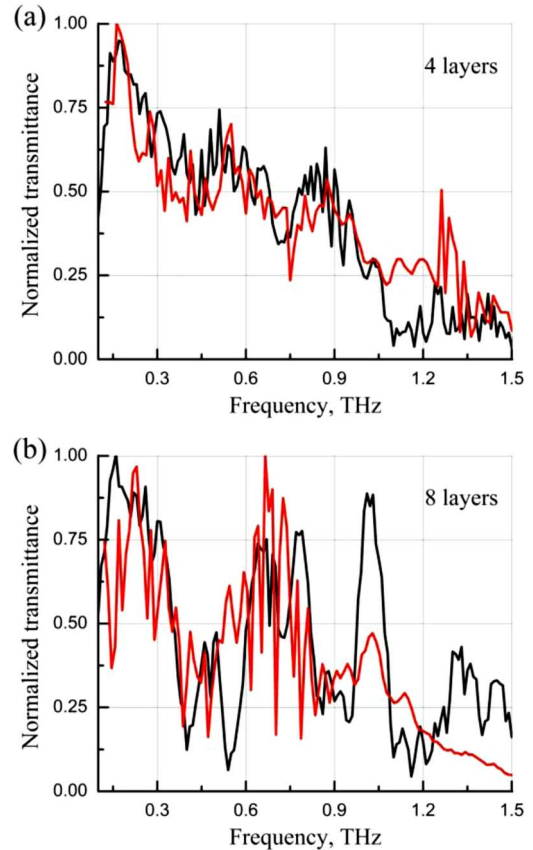

Fig. 8. Black line—normalized experimental transmittance, red line—theoretical normalized transmittance: (a) 4 layers waveguide, 11 cm length and (b) 8 layers waveguide, 11 cm length.

losses. Convenient access to the modal fields in the air regions and on the waveguide surface makes them useful for sensing of biological and chemical specimens in the THz region. The transmission and absorption properties of such waveguides have been investigated both experimentally using THz-TDS spectroscopy and theoretically using finite element software. Good agreement between experimental data and theoretical results has been achieved.

REFERENCES

[1] Y.-S. Jin, G.-J. Kim, and S.-G. Jeon, "Terahertz dielectric properties of polymers," *J. Korean Phys. Soc.*, vol. 49, no. 2, pp. 513–517, 2006.
[2] B. Ung, A. Mazhorova, A. Dupuis, M. Rozé, and M. Skorobogatiy, "Polymer microstructured optical fibers for terahertz wave guiding," *Opt. Express*, vol. 19, no. 26, pp. B848–B861, 2011.
[3] M. Roze, B. Ung, A. Mazhorova, M. Walther, and M. Skorobogatiy, "Suspended core subwavelength fibers: Towards practical designs for low-loss terahertz guidance," *Opt. Express*, vol. 19, pp. 9127–9138, 2011.
[4] L.-J. Chen, H.-W. Chen, T.-F. Kao, J.-Y. Lu, and C.-K. Sun, "Low-loss subwavelength plastic fiber for terahertz waveguiding," *Opt. Lett.*, vol. 31, no. 3, pp. 308–310, 2006.

[5] J. A. Harrington, R. George, P. Pedersen, and E. Mueller, "Hollow polycarbonate waveguides with inner Cu coatings for delivery of terahertz radiation," *Opt. Express*, vol. 12, pp. 5263–5268, 2004.

[6] B. Bowden, J. A. Harrington, and O. Mitrofanov, "Silver/polystyrene-coated hollow glass waveguides for the transmission of terahertz radiation," *Opt. Lett.*, vol. 32, pp. 2945–2947, 2007.

[7] T. Ito, Y. Matsuura, M. Miyagi, H. Minamide, and H. Ito, "Flexible terahertz fiber optics with low bend-induced losses," *J. Opt. Soc. Amer. B*, vol. 24, no. 5, pp. 1230–1235, 2007.

[8] A. Dupuis, K. Stoeffler, B. Ung, C. Dubois, and M. Skorobogatiy, "Transmission measurements of hollow-core THz Bragg fibers," *J. Opt. Soc. Amer. B*, vol. 28, pp. 896–907, 2011.

[9] C.-H. Lai, Y.-C. Hsueh, H.-W. Chen, Y.-J. Huang, H. Chang, and C.-K. Sun, "Low-index terahertz pipe waveguides," *Opt. Lett.*, vol. 34, pp. 3457–3459, 2009.

[10] C.-H. Lai, B. You, J.-Y. Lu, T.-A. Liu, J.-L. Peng, C.-K. Sun, and H. Chang, "Modal characteristics of antiresonant reflecting pipe waveguides for terahertz waveguiding," *Opt. Express*, vol. 18, pp. 309–322, 2010.

[11] A. Mazhorova, A. Markov, B. Ung, M. Rozé, S. Gorgutsa, and M. Skorobogatiy, "Thin chalcogenide capillaries as efficient waveguides from mid-IR to THz," *J. OSA B*, submitted for publication.

[12] R. Mendis and D. Grischkowsky, "Undistorted guided-wave propagation of subpicosecond terahertz pulses," *Opt. Lett.*, vol. 26, p. 846, 2001.

[13] M. Nagel, A. Marchewka, and H. Kurz, "Low-index discontinuity terahertz waveguides," *Opt. Express*, vol. 14, p. 9944, 2006.

[14] K. Wang and D. Mittleman, "Metal wires for terahertz guiding," *Nature*, vol. 432, p. 376, 2004.

[15] A. Mazhorova, A. Markov, A. Ng, R. Chinnappan, O. Skorobogata, M. Zourob, and M. Skorobogatiy, "Label-free bacteria detection using evanescent mode of a suspended core terahertz fiber," *Opt. Express*, vol. 20, no. 5, pp. 5344–5355, 2012.

[16] B. Scherger, M. Scheller, N. Vieweg, S. Cundiff, and M. Koch, "Paper terahertz wave plates," *Opt. Express*, vol. 19, pp. 24884–24889, 2011.

[17] M. Skorobogatiy, *Nanostructured and Subwavelength Waveguides: Fundamentals and Applications*.   Hoboken, NJ, USA: Wiley, 2012.

[18] A. Mazhorova, J. F. Gu, A. Dupuis, M. Peccianti, O. Tsuneyuki, R. Morandotti, H. Minamide, M. Tang, Y. Wang, H. Ito, and M. Skorobogatiy, "Composite THz materials using aligned metallic and semiconductor microwires, experiments and interpretation," *Opt. Express*, vol. 18, no. 24, pp. 24632–24647, 2010.

Andrey Markov was born in Troitsk, Russia, in 1986. He received the Diploma degree in physics from the Lomonosov Moscow State University in 2009, and is currently working towards the Ph.D. degree from the Ecole Polytechnique de Montreal, Canada.

He is a member of the Complex Photonic Structures and Processes Group of Prof. Maksim Skorobogatiy at the Ecole Polytechnique de Montreal, Canada. His current research involves modeling of microstructured waveguides for their applications in near-IR plasmonics, mid-IR guidance and THz.

Anna Mazhorova was born in Korolyov, Russia, in 1985. She received the Diploma degree in physics from the Lomonosov Moscow State University in 2009, and the Ph.D. degree from the Ecole Polytechnique de Montreal, Canada in 2012.

In 2009–2012, she was a member of the Complex Photonic Structures and Processes Group of Prof. Maksim Skorobogatiy at the Ecole Polytechnique de Montreal, Canada. Since 2012 she is a post-doctoral researcher in the Nonlinear Optics and Micro-and Nano-Structures for Photonics group of Prof. Roberto Morandotti at the Institut National de la Recherche Scientifique (INRS), Canada.

Maksim Skorobogatiy received B.Sc. degree in physics from the Rochester Institute of Technology, Syracuse, NY, USA, in 1995, M.Sc. degree in physics from the McGill University, Montreal, QC, Canada, and M.Sc. degree in electrical engineering from the Massachusetts Institute of Technology (MIT), Cambridge, MA, USA, in 1997 and 2000, respectively, and Ph.D. degree in physics from MIT in 2001.

Since 2003, he is heading a research group on Advanced Photonic Structures at the Ecole Polytechnique de Montreal, Montreal, QC, Canada.